Re-evaluation of the role of static stress triggering for aftershocks following the Ridgecrest earthquake sequence considering receiver plane uncertainty

GEOSCIENCES THE UNIVERSITY OF ARIZONA

Catherine Hanagan[1] Rick Bennett[1] Amanda Hughes[1]

[1]University of Arizona, Department of Geosciences

Corresponding Author: C. Hanagan @ ceh5464@email.arizona.edu

NSF

MOTIVATION

* Aftershocks can cause appreciable destruciton in already earthquake-weakened regions despite their relatively small magnitudes.
* Understanding what triggers aftershocks is crucial for evaluating seismic hazard following an earthquake.

BACKGROUND

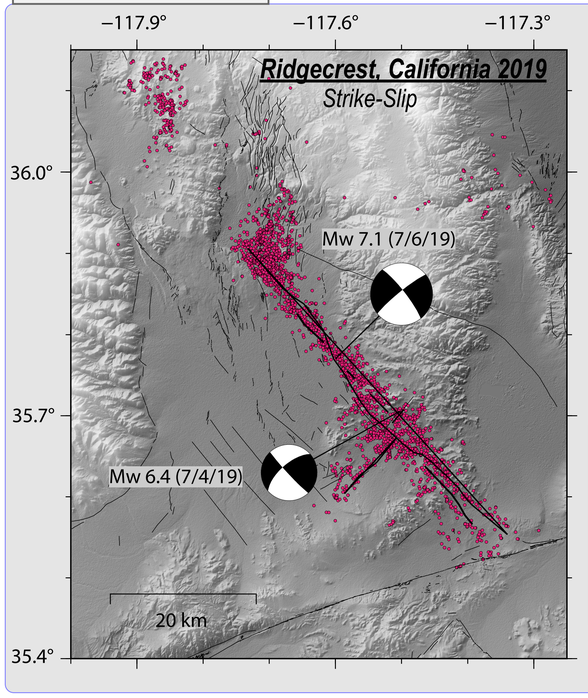

Mainshock-induced static stress transfer is commonly invoked as a mechanism for causing aftershocks, where coseismic stress changes encourage aftershock reciever planes toward failure; however, this hypothesis is subject to numerous uncertainties, hampering community consensus on its utility for aftershock hazard analysis. ***We use 2,889 aftershock focal mechanisms for three earthquake sequences to assess the static stress triggering hypothesis considering a full range of reciever plane uncertainty that has not been investigated to this extent in previous studies.***

Key Question: Can we discount mainshock-induced static stress triggering for any or all aftershocks after accounting for reciever plane location and orientation uncertainties?

Figure 1. Map of the 2019 Ridgecrest, California earthquake sequence study area. Aftershocks (maroon dots) are from the Lin (2020) catalogue. The bolded surface traces of the modelled coseismic slip distributions are from Ross et al. (2019). Mapped faults from the USGS quaternary fault database prior to the Ridgecrest rupture are presented as thin black traces, and moment tensors of the foreshock and mainshock are from the Caltech/USGS Southern California Seismic Network.

METHODS

1. Model static stress change from the largest earthquakes (Mw > 5.5; Figure 1).

2. Identify aftershock reciever planes for the published aftershock hypocentral locations.

Plane Categories

a) Optimally Oriented Planes (OOPs)
These are commonly used when focal mechanisms are not available. OOPs are conjugate planes chosen to maximize CFS in the combined deviatoric regional stress field and coseismic stress change field.

b) Focal Mechanism Planes. One nodal plane is chosen according to the categories:
(I) Lower ΔCFS (nodal plane in lower coseismic ΔCFS)
(II) Higher ΔCFS (nodal plane in higher coseismic ΔCFS)
(III) Reg+Eq Unstable (nodal plane in higher CFS for the regional and coseismic stress field)
(IV) Reg Unstable (nodal plane in higher CFS for the regional stress field)
(V) Strike Constrained (nodal plane best aligned with strikes of mapped faults)

2.1. Sample the location (x, y, z) and orientation (strike, dip, rake) parameters from joint normal distributions with standard deviations from the published datasets.

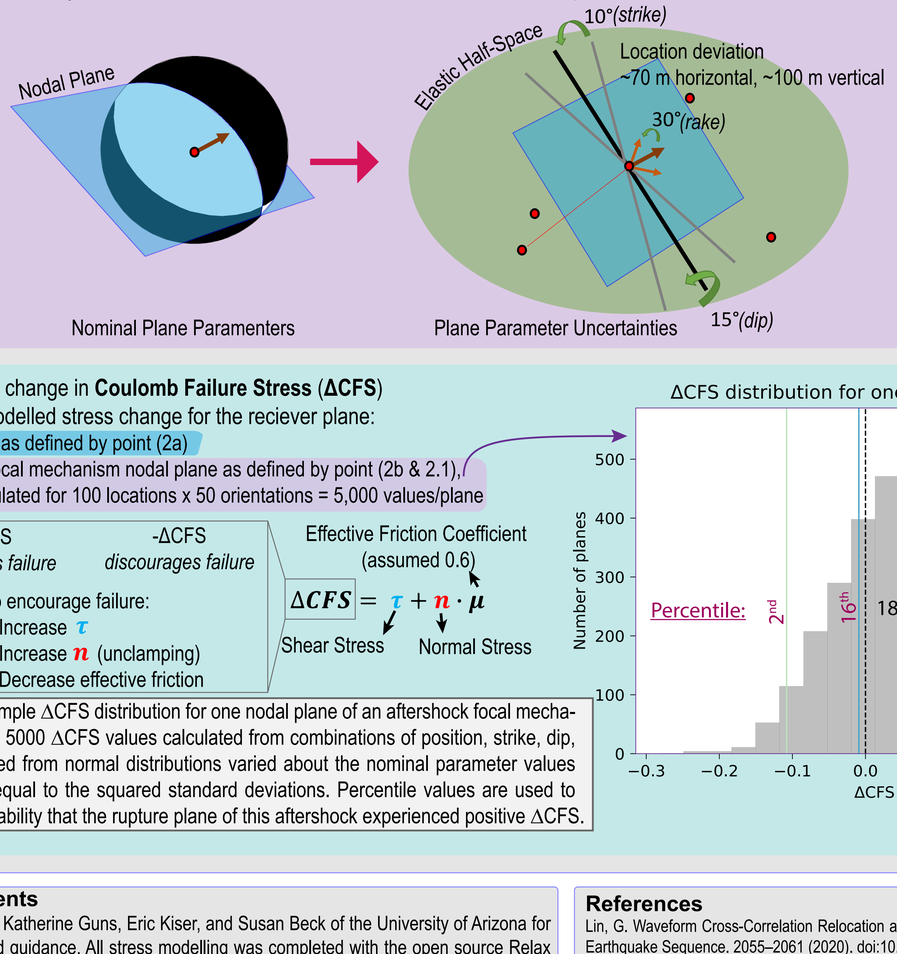

3. Evaluate the change in **Coulomb Failure Stress** (**ΔCFS**) using the modelled stress change for the reciever plane:
- For OOPs, as defined by point (2a)
- For each focal mechanism nodal plane as defined by point (2b & 2.1), this is calculated for 100 locations x 50 orientations = 5,000 values/plane

+ΔCFS *encourages failure* | -ΔCFS *discourages failure*

To encourage failure:
- Increase τ
- Increase n (unclamping)
- Decrease effective friction

Effective Friction Coefficient (assumed 0.6)

$$\Delta CFS = \tau + n \cdot \mu$$

Shear Stress | Normal Stress

Figure 2. Example ΔCFS distribution for one nodal plane of an aftershock focal mechanism, containing 5000 ΔCFS values calculated from combinations of position, strike, dip, and rake sampled from normal distributions varied about the nominal parameter values with variances equal to the squared standard deviations. Percentile values are used to assess the probability that the rupture plane of this aftershock experienced positive ΔCFS.

RESULTS

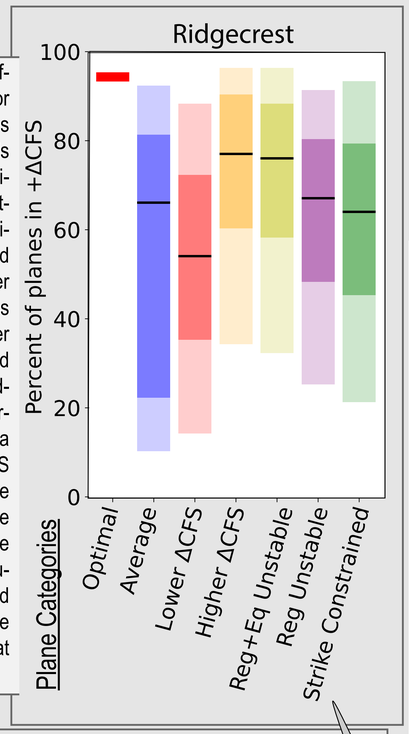

Figure 3. Percentages of aftershocks in positive ΔCFS for OOPs (red bar) and categories of nodal planes (see methods section). The black bars indicate the percentage of promoted aftershocks given the nominal nodal plane orientation and location values. The darker colored regions encompass the 1σ percentage range after incorporating orientation and location uncertainties, bounded on the lower end by the percentage of aftershocks with a positive 16th percentile ΔCFS distribution value, and on the upper end by the percentage of aftershocks with a positive 84th percentile ΔCFS distribution value. The lighter colored regions are the 2σ percentage ranges, similarly defined but at the 2nd and 98th percentiles.

What is the structure of the aftershock planes?

Table 1. Average minimum angular difference between normal and slip vector orientations for OOPs and nodal planes of an aftershock.

OOPs vs Nodal Planes	Ridgecrest
Normal vector difference	33.8°
Slip vector difference	45.6°

OOPs do not match observed planes from focal mechanisms!

The strike constraint best reproduces observations of mapped fault strikes.

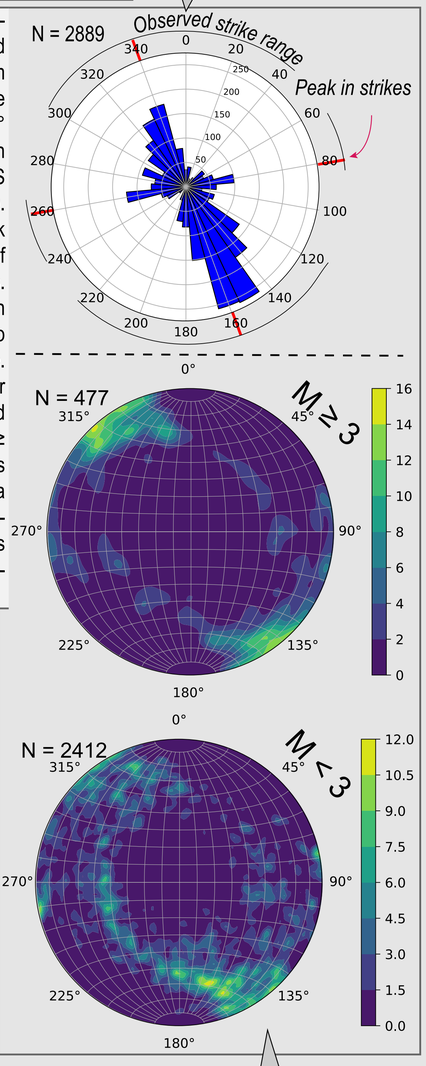

Figure 4. (**Top**) Rose diagram of the strike constrained nodal planes. The diagram contours are labelled for the number of events in each 10° bin. Red lines mark peaks in mapped fault strikes (USGS Qfaults database in Figure 1). Thin circumferential black lines represent the range of strikes from mapped faults. Note that 180° differences in strike have no meaning for dip direction of the fault plane. (**Bottom**) Slip vector contour plots for the strike constrained nodal planes separated by M≥ 3 and M<3. The slip vectors are presented in equal-area projections with 2σ Kamb contouring. Number of slip vectors in each color contour are labelled to the right..

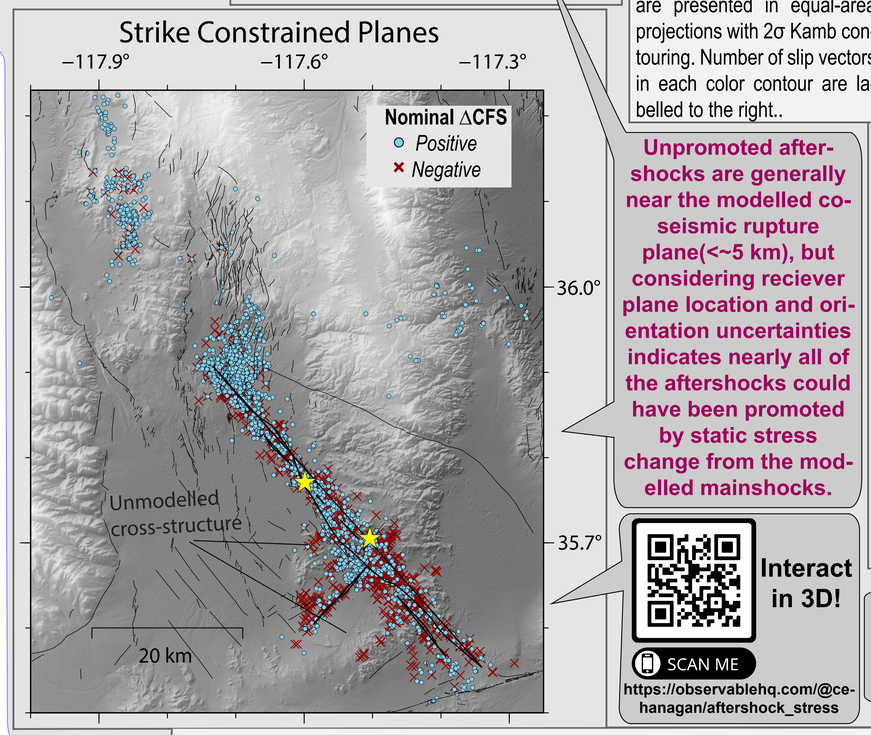

Unpromoted aftershocks are generally near the modelled coseismic rupture plane(<~5 km), but considering reciever plane location and orientation uncertainties indicates nearly all of the aftershocks could have been promoted by static stress change from the modelled mainshocks.

Interact in 3D!

SCAN ME

https://observablehq.com/@cehanagan/aftershock_stress

Generally, larger magnitude aftershocks slip with expected kinematics, while smaller magnitude aftershocks show more heterogeneous slip directions.

Figure 5. Aftershocks in positive ΔCFS (blue circle) and negative ΔCFS (red cross) for strike constrained nodal planes. Yellow stars mark the hypocenters of the modelled earthquake ruptures. Aftershocks, slip distribution outlines, and fault traces are the same as in Figure 1. Many unpromoted aftershocks lie near the rupture plane. Unmodelled orthogonal faults host many unpromoted events.

Discussion+Conclusion

KEY FINDINGS

Key Conclusion:

We cannot discount static stress triggering for nearly all of the aftershocks after considering reciever plane uncertainties.

+ Static stress change from the largest mainshocks nominally encourages ~65% of the aftershocks toward failure.
+ OOPs overestimate the role of static stress triggering, and misrepresent the orientations of aftershock rupture planes.
+ The percentage of triggered events markedly increases (by ~20%) in the far-field, greater than 5 km from the coseismic rupture planes.
+ The aftershocks align best in strike with pre-existing mapped surface faults, though the plane orientations and slip directions of smaller magnitude events (M<3) are more heterogeneous.
+ The orientation uncertainty of focal mechanism planes, the problem of nodal plane ambiguity, and, to second order, the location uncertainty expand the 1σ percentage range for the percentage of triggered aftershocks over 30%. The 2σ percentage range suggests nearly all of the observed aftershocks could have been triggered by static stress change.

CONCLUSION

Typically, failure of the static stress triggering hypothesis to explain aftershock occurrence is attributed to mis- or un-modelled fault zone processes, particularly within 5 km of the modelled rupture planes. We demonstrate that uncertainty in the receiver planes is equally, or potentially more, important to consider. This earthquake sequence was studied in conjunction with the 1997 Umbria-Marche and 2009 L'Aquila, Italy earthquake sequences, which corroborate the findings presented here. A better understanding of focal mechanism orientation errors and the structure of smaller-scale faults in the crust could tighten estimates on the role of static triggering. Nonetheless, the correspondence of our nominal results in combination with past analyses of the static stress triggering hypothesis indicates over half of the aftershocks are promoted by static stress change, with more common estimates nearing two-thirds of promoted aftershocks, regardless of magnitude. Near the modelled ruptures, high uncertainty and/or other triggering processes may explain events that remain unlikely to fail.

Acknowledgements

We would like to thank Katherine Guns, Eric Kiser, and Susan Beck of the University of Arizona for helpful discussions and guidance. All stress modelling was completed with the open source Relax software of the Computational Infrastructure for Geophysics, for which Sylvain Barbot provided helpful support. This study focuses on one of three similarly studied earthquake sequences, for the other seqeunces in Italy, Lauro Chiaraluce and Massimo Cocco provided insightful discussion and guidance that enter into the conclusions drawn here.This material is based upon work supported by the National Science Foundation under Grant No. 1723045.

References

Lin, G. Waveform Cross-Correlation Relocation and Focal Mechanisms for the 2019 Ridgecrest Earthquake Sequence. 2055–2061 (2020). doi:10.1785/0220190277.

Ross, Z. E. et al. Hierarchical interlocked orthogonal faulting in the 2019 Ridgecrest earthquake sequence. Science (80-.). 366, 346–351 (2019).

Wessel, P., Luis, J. F., Uieda, L., Scharroo, R., Wobbe, F., Smith, W. H. F., & Tian, D. (2019). The Generic Mapping Tools version 6. Geochemistry, Geophysics, Geosystems, 20, 5556–5564. https://doi.org/10.1029/2019GC008515